Journal of Applied Polymer Science

Cell evolution and compressive properties of styrene–butadiene–styrene toughened and calcium carbonate reinforced polystyrene extrusion foams with supercritical carbon dioxide

Xin Jing,[1] Xiang-Fang Peng,[1] Hao-Yang Mi,[1] Yuan-Sheng Wang,[1] Shuidong Zhang,[2] Bin-Yi Chen,[2] Hua-Min Zhou,[3] Wen-Jie Mou[2,3]

[1]Key Laboratory of Polymer Processing Engineering (Ministry of Education), South China University of Technology, Guangzhou 510640, China

[2]Department of Industrial Equipment and Control Engineering, South China University of Technology, Guangzhou 510640, China

[3]State Key Laboratory of Materials Processing and Die & Mold Technology, Huazhong University of Science and Technology, Wuhan 430074, China

Correspondence to: H.-Y. Mi (E-mail: mehymi@scut.edu.cn) and W.-J. Mou (E-mail: wjmou@scut.edu.cn)

ABSTRACT: Polystyrene (PS) foams have been used in various fields, whereas its broader application is limited by its low mechanical strength and brittle features. In this study, styrene–butadiene–styrene (SBS) and calcium carbonate ($CaCO_3$) nanoparticles were melt-blended with PS and extrusion-foamed with supercritical carbon dioxide as a blowing agent to simultaneously toughen and reinforce PS foams. Under the same foaming conditions, the addition of SBS and $CaCO_3$ was shown to have a significant influence on the cell structure and the compressive properties of the composite foams. We found that the cell structure evolution was highly correlated with the system viscosity. When the rubbery-phase SBS content was 20%, the cell diameter decreased by 20.7%, and the compressive modulus was enhanced by 289.5%. With the further addition of 5% rigid $CaCO_3$ nanoparticles, the cell diameter was further reduced by 72.2% and the compressive modulus was improved by 379.2%. © 2016 Wiley Periodicals, Inc. J. Appl. Polym. Sci. **2016**, *133*, 43508.

KEYWORDS: extrusion; foams; mechanical properties; porous materials

Received 9 November 2015; accepted 3 February 2016
DOI: 10.1002/app.43508

INTRODUCTION

Polymer foams with cell sizes within 100 μm are known to exhibit many advantages over unfoamed materials; these advantages include a lower weight, higher impact strength,[1,2] higher toughness,[3] higher stiffness-to-weight ratio,[4] higher fatigue life,[5] lower thermal conductivity,[2] and higher sound insulation.[6] Because of these excellent properties, polymer foams have been used in many applications, including automobiles, aircraft, packing materials, thermal insulation, transportation, structural components, and medical devices.[7–9] As the market demand for polymer foams increases, the need for a method to efficiently produce polymer foams with good properties has become pronounced and has attracted more and more attention in recent years. Chemical foaming agents are commonly used in various foaming methods. However, these may cause pollution and product impurity, which limit the products' applications. Physical blowing agents, such as supercritical carbon dioxide ($SC\text{-}CO_2$) and nitrogen, can induce microcells within the polymer matrix by gas expansion. They are environmentally friendly, economic, and highly appreciated in many applications. Various foaming methods, such as batch foaming, microcellular injection molding, and extrusion foaming, use physical blowing agents to produce polymer foams. Among these methods, extrusion foaming, which can continuously produce polymer foams with uniform microcells, has the highest productivity and the lowest cost. Extrusion foaming has been used to produce different kinds of polymer foams, and the effects of the extrusion foaming parameters (i.e., screw rotation speed, gas content, foaming temperature) on the cell morphology have been studied extensively.[10,11]

Polystyrene (PS) is a commonly used polymer in industry and construction fields. However, the brittleness of PS limits its wide application. The toughening of PS through the addition of a rubbery phase has been a hotspot for many years. Natural rubber[12,13] and styrene–butadiene–rubber[14] have been applied into the PS matrix to modify the properties of PS, especially its rigid mechanical attributes. Poly(styrene–butadiene–styrene) triblock copolymers ease the process and have unique

© 2016 Wiley Periodicals, Inc.

characteristics that are similar in many ways to those of conventional vulcanized rubber.[15] It has been reported that the phase boundary,[16] relaxation behavior,[17] thermal properties,[15] and mechanical properties[18] of PS were different after it was mixed with styrene–butadiene–styrene (SBS). The addition of SBS improved the impact strength of the PS/SBS system significantly, whereas the tensile strength and tensile modulus were dramatically reduced at the same time.[19,20] Even though the properties of the PS/SBS blends were investigated, so far there has been no literature on the extrusion foaming behavior of the PS/SBS system via a physical blowing agent, and study of the mechanical performance of PS/SBS microcellular foams is still lacking.

Moreover, nanoparticles, such as organophilic layered silicates,[21] metal oxides,[22] and carbon nanotubes,[23] were also used to blend with PS to improve its thermal and mechanical properties (e.g., thermal stability, stiffness, strength, creep-resistance properties).[24,25] The compounding of PS with both rubber and rigid nanoparticles has attracted considerable attention because of the promise of simultaneous improvements in the stiffness and toughness.[26] It has been shown that bentonite clay could compatibilize and reinforce the natural rubber/PS system via a latex blending process.[27] The addition of boehmite alumina into the PS/styrene–butadiene–rubber system was found to produce toughened and reinforced polymer composites.[28] Calcium carbonate ($CaCO_3$) nanoparticles are often used as fillers in composite materials as crystallization nucleation agents or reinforcing additives.[29,30] These nanoparticles would be promising additives to the PS/SBS system. With respect to the microcellular foaming, $CaCO_3$ is a commonly used nucleation agent that can induce cell nucleation and improve cell density during the foaming process. This effect has been reported in PS SC-CO_2 foaming.[31] However, there have been no reports on the foaming behavior of the PS/SBS/$CaCO_3$ ternary system. It is worth investigating the cell nucleation and reinforcing effects of $CaCO_3$ nanoparticles on the foaming behavior and mechanical performance of PS/SBS/$CaCO_3$ nanocomposites.

In this study, PS/SBS binary and PS/SBS/$CaCO_3$ ternary composites were prepared via a triple-screw extruder. The phase morphology and rheological properties of the systems were investigated to further elaborate their extrusion foaming behaviors. The effects of the SBS and $CaCO_3$ nanoparticles on the cell diameter and cell density were demonstrated in detail. The compressive properties of the foamed blends and nanocomposites were studied to investigate the correlations among the material combination, cell structure, and mechanical properties.

EXPERIMENTAL

Materials

PS (N1841H), with a melt flow index of 8 g/10 min according to ASTM D 1238 and a density of 1.04 g/cm^3, was purchased from Hong Kong Petrochemical Co., Ltd. SBS (YH-792), whose S/B ratio was 40:60, was purchased from China Petroleum & Chemical Co. Nanosized $CaCO_3$ was supplied by Jia Wei Chemical industrial Co., Ltd., with an average size around 80 nm and a density of 2.5 g/cm^3. Commercial purity-grade CO_2 (purity = 99%, Air Liquid, Jinzhujiang Chemical Co.) was used as a physical blowing agent in the extrusion foaming process.

Preparation of the PS/SBS Blends and PS/SBS/$CaCO_3$ Nanocomposites

PS/SBS blends with SBS proportions of 5, 10, 15, and 20% were prepared with a triple-screw extruder (IEGTC-25/40, Guangzhou POTOP Co., Ltd., China) equipped with a screw 25 mm in diameter with a length-to-diameter ratio of 40. The temperature profile was set at 160 °C in the feed zone, sequentially at 165, 170, 175, 180, 180, 180, 175, and 170 °C in the metering zone, and 170 °C at the die. The feeding rate and triple-screw rotation speed were set at 7 and 50 rpm, respectively. The extrudate was cooled via water cycling and granulated with a pelletizer. The PS/SBS/$CaCO_3$ nanocomposites were prepared by the addition of $CaCO_3$ nanoparticles into the PS/SBS blends with 20% SBS. The process and parameters were the same as those used for the preparation of the PS/SBS blends. A series of nanocomposites with $CaCO_3$ concentrations of 1, 3, 5, and 10% were obtained.

Extrusion Foaming Process

Extrusion foaming of the neat PS, PS/SBS blends, and PS/SBS/$CaCO_3$ nanocomposites were carried out on a single-screw extruder (diameter = 45 mm, length/diameter ratio = 29) with a die diameter of 1.5 mm and length-to-diameter ratio of 10; the extruder was equipped with a supercritical gas supply system (ISCO-260D). The processing temperature profile used was 165, 180, 165, and 150 °C from the hopper to the extrusion die, and the screw rotating speed was 13 rpm. These processing parameters were optimized on the basis of our single-screw extrusion foaming system, and the same processing conditions were used for all of the experimental groups to prevent side effects from the parameters. During the process, SC-CO_2 was pumped into the middle section of the metering zone and mixed with the polymer melt by screw rotation. The extrudate was foamed once they exited the die, where the blowing agent turned from supercritical state into a gas state. The extruded foams were cooled in air and collected as foamed strings with a diameter of about 8 mm.

Characterization

The phase morphology of the PS/SBS blends and the dispersion of $CaCO_3$ particles in the nanocomposites were observed via scanning electron microscopy (SEM; MERLIN, Zeiss) with high magnification. The samples used were the extrudate from the triple-screw extruder. The cell structure of the extrusion-foamed samples were imaged with the same SEM instrument at lower magnification. All samples were submerged in liquid nitrogen and cryofractured in the cross section and sputtered with a thin film of gold before imaging.

The mean cell diameter and cell density statistical results were determined from the SEM micrographs with Image Pro-Plus software. The cell density (N_0) was calculated according to the following equation:

$$N_0 = \left(\frac{n}{A}\right)^{3/2} \quad (1)$$

where n is the number of cells in the SEM micrograph and A is the measured area of the SEM image. The values are the average of three samples.

To investigate the rheological properties of the PS/SBS blends and PS/SBS/$CaCO_3$ nanocomposites, a Bohlin Gemini 200 Rheometer (Bohlin, Ltd., Worcestershire, United Kingdom) equipped with a parallel-plate fixture (25 mm in diameter) was used in an oscillatory mode to conduct dynamic frequency sweep tests. The complex viscosity (η), storage modulus (G'), and loss modulus (G'') as a function of the angular frequency (ω), which ranged from 0.01 to 100 rad/s, were measured at 180 °C. A fixed strain of 1% was used to ensure that the measurements were carried out within the linear viscoelastic range.

Differential scanning calorimetry (DSC) analysis was performed with a DSC instrument (204 F1, Netzsch, Germany) to study the effect of SBS on the thermal properties of PS and their miscibility. The samples were weighed and loaded in standard aluminum pans and placed in the DSC cell. They were first heated from room temperature to 200 °C at 10 °C/min, kept for 3 min to eliminate the thermal history, and subsequently cooled to 20 °C at 10 °C/min. This was followed by heating again to 200 °C at 10 °C/min. This second heating process was regarded as a melting scan for the analysis.

The impact and tensile properties of the PS/SBS blends were evaluated in this study. The tensile test was carried out on a universal testing system (Instron5566) with ISO standard specimens ($150 \times 20 \times 4\ mm^3$) machined by injection molding. The crosshead speed was 5 mm/min. Izod impact tests were carried out on a POE200 pendulum impact testing machine (Instron Co.) with ISO standard specimens ($80 \times 10 \times 4\ mm^3$, notch depth = 2 mm) also machined by injection molding. At least five specimens were tested for each group.

Compression tests of the foamed samples were carried out on an Instron 5566 compression test machine. The extruded strings were cut into cylinders (ca. 5–8 mm in diameter and 10 mm in height) and compressed at ambient temperature with a crosshead speed of 1 mm/min. Strain–stress curves were recorded, and 40% strain was set as the termination of the test.

RESULTS AND DISCUSSION

Properties of PS/SBS Blends

Miscibility and Phase Morphology of PS/SBS Blends. The PS/SBS blends were prepared by melt compounding via a triple-screw extruder to achieve homogeneous mixing. The miscibility and interphase of the components are the most important factors determining its properties.[32] In this study, the miscibility was studied by DSC, and the second heating thermograms are shown in Figure 1. We found that instead of showing two distinct glass-transition temperatures, the glass-transition temperature of PS shifted to a higher temperature when the content of SBS increased; this indicated that SBS was compatible with the PS matrix and that the thermal properties of PS were altered by the addition of SBS. This finding was consistent with a previous study on the gradient interfaces in PS/SBS blends.[20]

Figure 2 shows the morphology of the cryofractured surfaces of the PS and PS/SBS blends and the effect of the SBS content on the phase morphology of PS/SBS blends. The neat PS [Figure 2(a)], 5% SBS [Figure 2(b)], and 10% SBS [Figure 2(c)] samples showed relative smooth fractured surfaces without presenting obvious phase separation. This indicated good compatibility between the PS and SBS components. Although we found that the blends still showed typical brittle fractured surfaces, similar to neat PS. However, when the SBS content was greater than 15%, the cryofractured surfaces became rough and uneven. This was because the toughness of the material was improved by the added SBS; this resulted from the rubbery properties of SBS. During cryofracturing, SBS was highly stretched under an external force; this resulted in the formation of a rough-phase morphology, which corresponded to an obvious improvement of SBS on the impact properties of PS in the previous studies.[19,33]

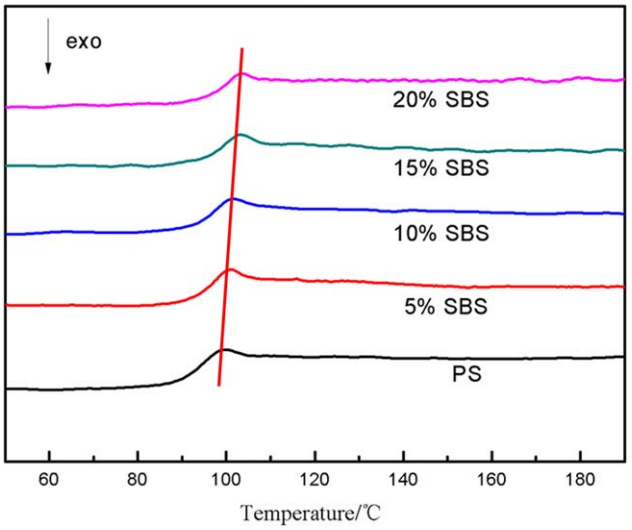

Figure 1. DSC thermograms of the PS and PS/SBS blends in the second heating cycle. [Color figure can be viewed in the online issue, which is available at wileyonlinelibrary.com.]

Toughening Effect of SBS on PS. SBS was added to the PS matrix to overcome the brittle nature of PS. The mechanical properties of the PS/SBS blends are shown in Figure 3. According to these results, one can clearly see that the impact strength [Figure 3(a)] and elongation at break [Figure 3(c)] of the blends were enhanced dramatically as the content of SBS increased in the PS matrix; this indicated the toughening effect of SBS because of its rubbery property. However, from the tensile test results, we found that the stiffness of the blends, as presented by the tensile modulus and tensile strength, was reduced significantly when the SBS content was increased. This phenomena is quite normal in rubber-toughened material systems, in which the rubbery phase consumes and stores energy in mechanical deformation and preventing material from failure. At the same time, the strength and modulus of the material decreases. Similar results have been reported elsewhere.[33]

Rheological Properties of the PS and PS/SBS Blends. The rheological properties of polymers affect their foaming behavior significantly because foaming with a physical blowing agent is a result of the competition between the expansion force from the gas and the surface tension of the polymer matrix. Figure 4 shows the G', G'', and η values of the PS and PS/SBS blends. We found that G' [Figure 4(a)] increased with increasing SBS content in the blends, in particular for the 15 and 20% SBS

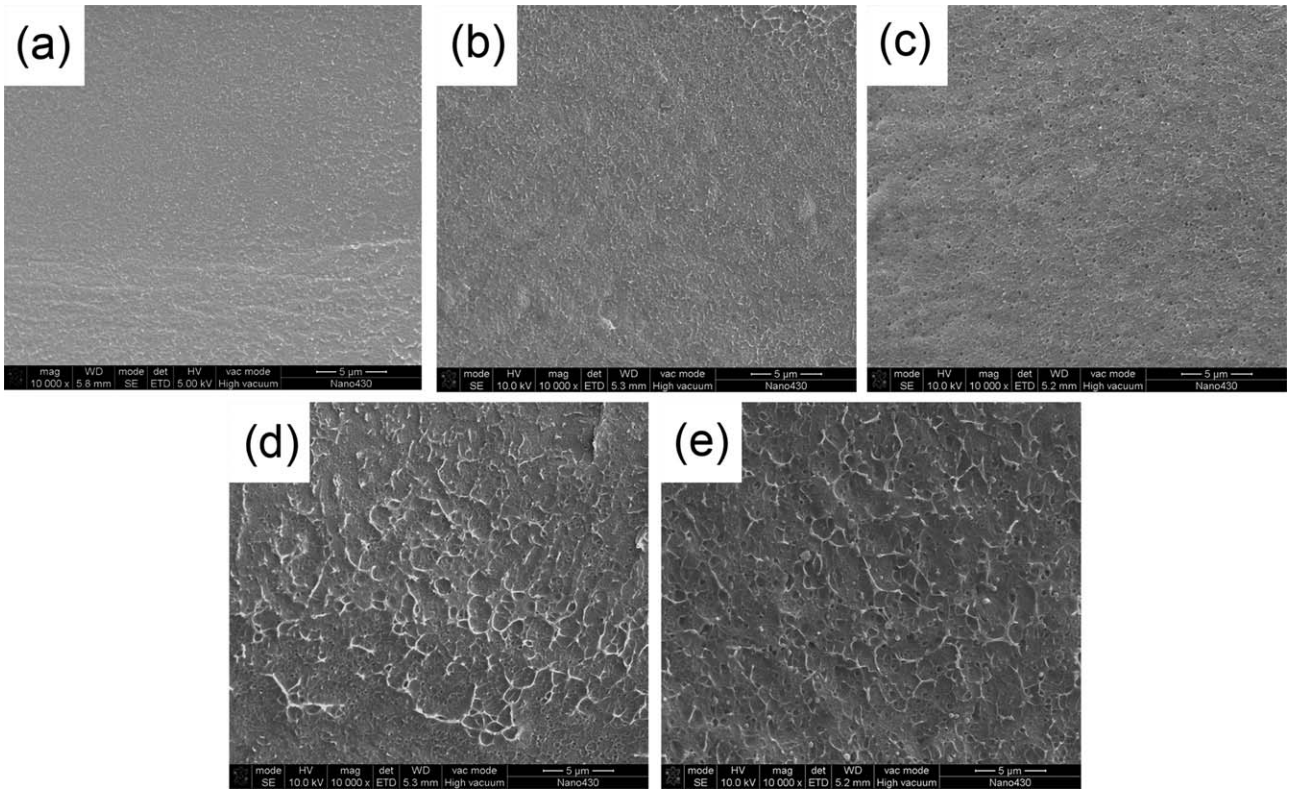

Figure 2. Phase morphologies of the (a) PS, (b) 5% SBS, (c) 10% SBS, (d) 15% SBS, and (e) 20% SBS.

samples, and the improvement was much more significant at low ω. This indicated an improvement in the elasticity or rubbery property; this was in accordance with the observations from the phase morphology results. According to Figure 4(b), G'' was also slightly enhanced with increasing SBS, whereas the improvement was less marked. This indicated that the added SBS did not enhance the plasticity largely. Figure 4(c) shows that the viscosity of 5 and 10% SBS was slightly lower than that of the neat PS at low frequency, whereas it was higher than that of the neat PS at high frequency. As shown by the fractured phase morphology in Figure 2, the 5 and 10% SBS samples showed flat surfaces; this may have indicated low interfacial activity between the SBS and PS or no SBS network formed in the PS matrix. As the frequency increased, the SBS phases were deformed and interconnected to form a network; this contributed to the improvement in the viscosity. Noticeably, the viscosities of the 15 and 20% SBS samples were much higher at low ω than those of the others. This proved that when the SBS content exceeded a certain value, it could form an interconnected network in the PS matrix and induce a significant improvement in the system viscosity. These results imply that the viscosity of the PS/SBS blends relied highly on the proportion of SBS. The viscosity difference was consistent with the phase morphology results; this affected the extrusion foaming behavior of the PS/SBS blends.

Extrusion Foaming Morphologies of the PS and PS/SBS Blends

The cell morphologies of the extruded PS and PS/SBS are shown in Figure 5. With these results, we found that all of the samples formed a highly porous structures, even though the cell sizes were different. The mean cell diameter and cell density

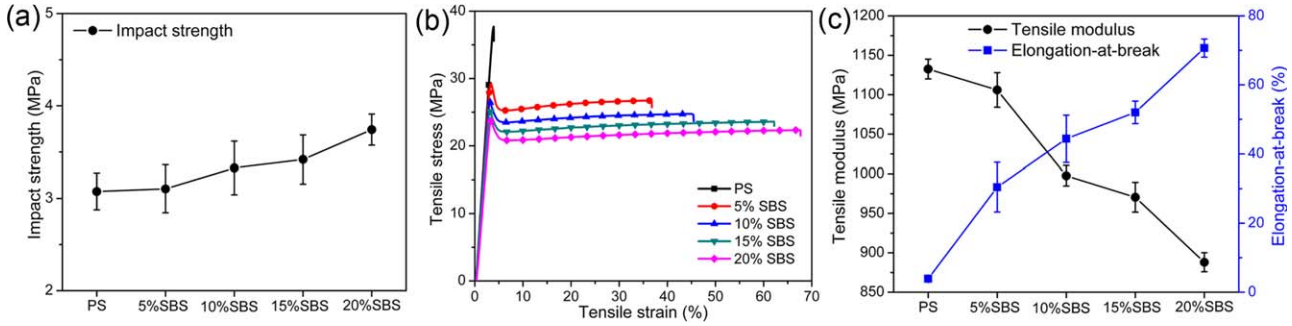

Figure 3. (a) Impact strength, (b) representative tensile test curves, and (c) tensile test statistical results for the PS and PS/SBS blends. [Color figure can be viewed in the online issue, which is available at wileyonlinelibrary.com.]

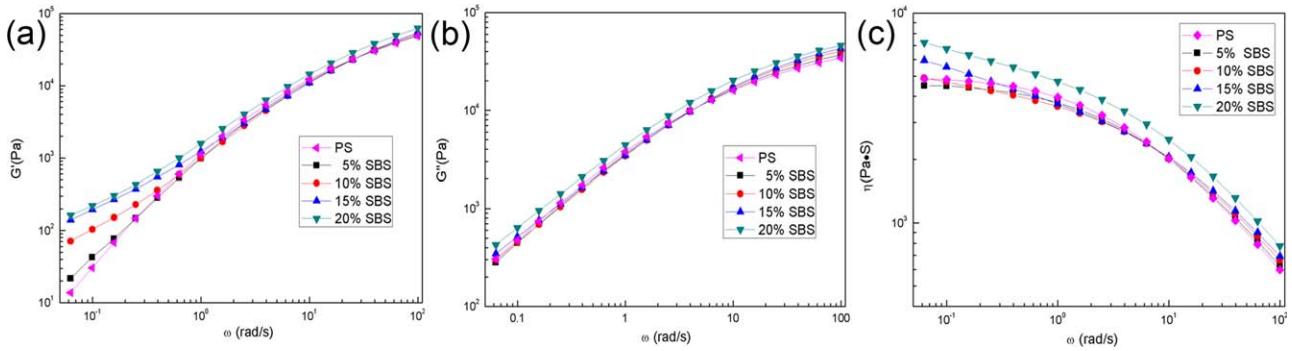

Figure 4. Rheological test results for the PS and PS/SBS blends: (a) G', (b) G'', and (c) η. [Color figure can be viewed in the online issue, which is available at wileyonlinelibrary.com.]

statistical results are shown in Figure 6. Combining these results, we found that the mean cell diameters of the 5 and 10% SBS samples were greater than that of the neat PS, whereas those of the 15 and 20% SBS samples were lower than that of the neat PS, and the mean cell density results show the opposite trends. Typically, the addition of another kind of polymer would enhance cell nucleation during foaming because of the heterogeneous nucleation boundaries created by the interphase between the two components.[34] However, for the PS/SBS blends, the rheological properties were the dominant factor for the foaming behavior because the PS and SBS showed good miscibility, and there were no obvious interphases (recall Figure 2). At low SBS contents, the system viscosity was lower; this resulted in a larger cell size and smaller cell density. On the contrary, when the SBS content was high, the viscosity of the blends increased; this led to a reduction in the cell size and an increase in the cell density. This was because the expansion force for cell growth became larger when the polymer system viscosity was high; this caused difficulty for cell formation and expansion. Because the extrusion foaming process was conducted at a low shear force, the cell morphology of the PS/SBS binary blends foams was in good agreement with the rheological results at low ω.

Dispersion of $CaCO_3$ and the Rheological Properties of the PS/SBS/$CaCO_3$ Nanocomposites

The combination of two different polymers produced polymer blends that possessed comprehensive properties of the components. When rigid nanofillers are added, they generally increase the mechanical properties of the substrate and its foaming properties by acting as nucleation agents.[35] In this study, nanosized $CaCO_3$ was used to further modify the properties of the PS/SBS blends and fabricate PS/SBS/$CaCO_3$ nanocomposite foams with a finer cell morphology. According to the previous results, the 20% SBS foams showed the smallest mean cell diameter and highest cell density. Therefore, 20% SBS was chosen as

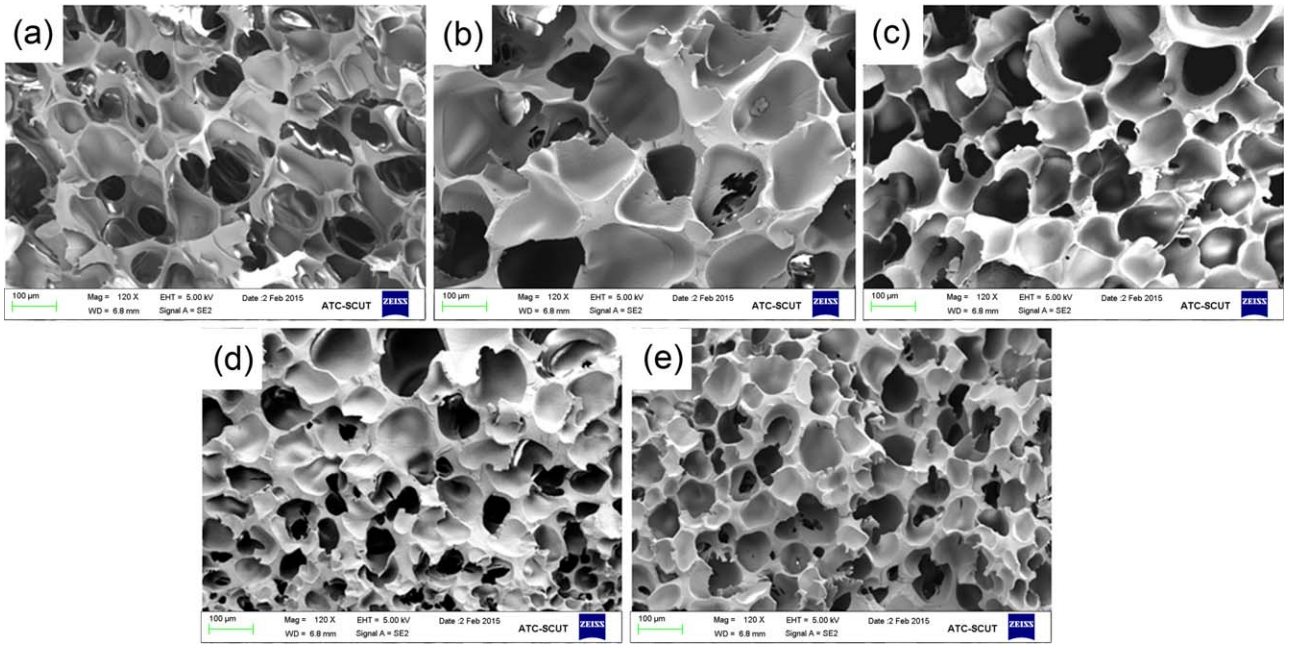

Figure 5. SEM images of extrusion-foamed samples: (a) PS, (b) 5% SBS, (c) 10% SBS, (d) 15% SBS, and (e) 20% SBS. [Color figure can be viewed in the online issue, which is available at wileyonlinelibrary.com.]

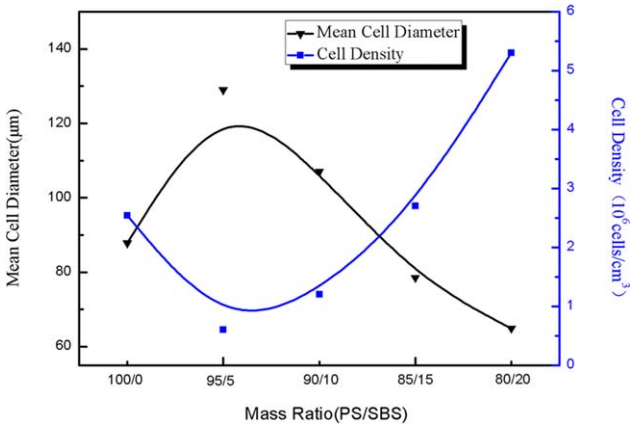

Figure 6. Statistical results for the mean cell diameter and cell density of the PS and PS/SBS blends. [Color figure can be viewed in the online issue, which is available at wileyonlinelibrary.com.]

the matrix in the following study to investigate the effect of $CaCO_3$. We varied the content of nanosized $CaCO_3$ particles from 1 to 10 wt % of the matrix to investigate the effect of $CaCO_3$ on the properties and extrusion foaming behavior of the PS/SBS blends.

Figure 7 shows the cryofractured surface of the PS/SBS/$CaCO_3$ nanocomposites with various $CaCO_3$ loading levels. We noticed that the $CaCO_3$ nanoparticles achieved good dispersion at low loading levels (i.e., 1 and 3%). As the content of $CaCO_3$ was further increased, more aggregated particle clusters were observed, as indicated by the red cycles in the SEM images, especially for the 10% $CaCO_3$ sample. The dispersion of nanofillers was a crucial factor that determined the final properties of the nanocomposites because the aggregated clusters reduced the surface-to-volume ratio of the particles and acted as stress-concentration points for the polymer matrix and caused early failure of the polymer under external force.

The rheological property test results of the PS/SBS/$CaCO_3$ nanocomposites are shown in Figure 8. We found that the addition of $CaCO_3$ significantly increased the rheological properties of the PS/SBS blends. Both G' [Figure 8(a)] and G'' [Figure 8(b)] were improved significantly after the addition of $CaCO_3$ particles; this represented the simultaneous improvement of elastic and plastic properties of the matrix. However, we noticed that the improvement effect became slight when the $CaCO_3$ loading level was 5%. G' and G'' were even reduced when the $CaCO_3$ loading level reached 10% at low ω. These variations were attributed to the increase in the $CaCO_3$ nanoparticle aggregation effect as its loading level increased. The η results in Figure 8(c) show a similar trend. The viscosity of the 1% $CaCO_3$ sample was much higher than that of the PS/SBS sample, and the improvement gradually decreased with increasing $CaCO_3$ loading level. The 10% $CaCO_3$ sample showed a lower viscosity than the 5% $CaCO_3$ sample. These results indicate that the amount of both individual nanoparticle $CaCO_3$ particles and $CaCO_3$ aggregates increased as the $CaCO_3$ loading level

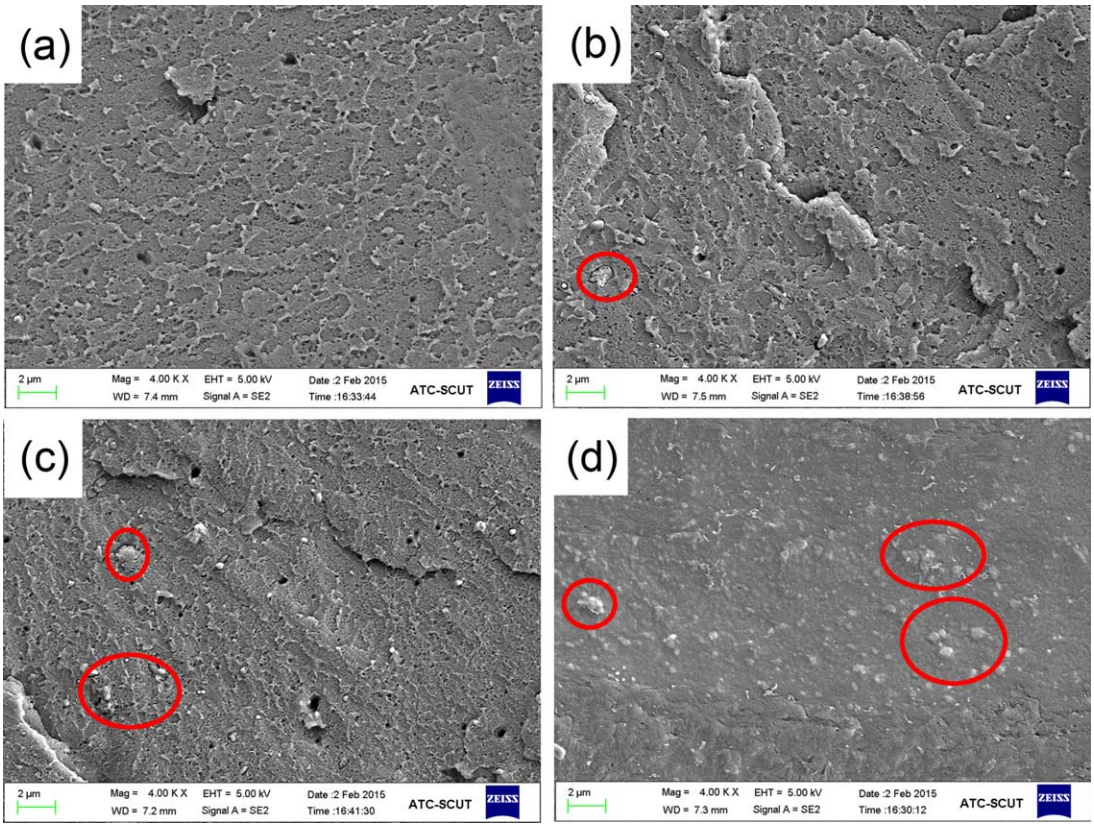

Figure 7. Phase morphologies of the (a) 1% $CaCO_3$, (b) 3% $CaCO_3$, (c) 5% $CaCO_3$, and (d) 10% $CaCO_3$. [Color figure can be viewed in the online issue, which is available at wileyonlinelibrary.com.]

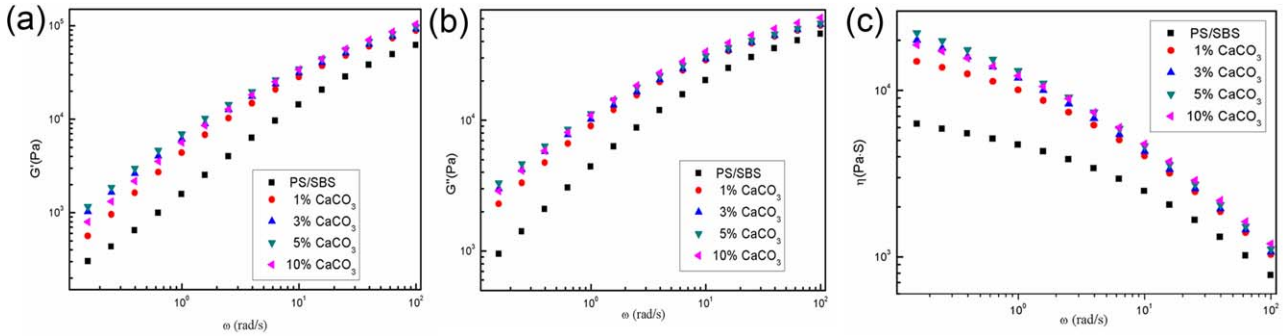

Figure 8. Rheological test results for the PS/SBS and PS/SBS/$CaCO_3$ nanocomposites: (a) G', (b) G'', and (c) η. [Color figure can be viewed in the online issue, which is available at wileyonlinelibrary.com.]

increased. Above the critical value, the defects from the $CaCO_3$ aggregates surpassed the benefits from the $CaCO_3$ nanoparticles; this led to a deteriorated performance in the nanocomposites in the rheological tests.

Extrusion Foaming Morphology of the PS/SBS/$CaCO_3$ Nanocomposites

Nanosized $CaCO_3$ particles have been widely used as nucleation agents in different foaming process because of their large specific surface area and high surface energy.[36] With the addition of $CaCO_3$ nanoparticles, there will be additional particle-matrix interphases; these reduce the cell nucleation energy barrier when the physical blowing agent evolves from a supercritical state into a gas state during depressurization. This results in a smaller cell size, a higher cell density, and normally, a superior mechanical performance.[37] In this study, nanosized $CaCO_3$ particles were introduced into the PS/SBS system as nucleation agents during the extrusion foaming process to improve the foaming and mechanical properties of the foams.

Figure 9 shows the cell morphologies of the PS/SBS/$CaCO_3$ nanocomposite foams with different $CaCO_3$ contents. We observed that the cells were distributed uniformly across the whole cross section, and they were compacted with relatively thin cell walls, with some of them even connecting with others because of the ruptured cell walls. Figure 10 shows the mean cell diameter and cell density statistical results of the foams. The mean cell diameter gradually increased, and the cell density decreased as the $CaCO_3$ content increased. Moreover, we noticed that the cell density increased from 2.54×10^6 cells/cm^3 for the PS foam to 5.3×10^6 cells/cm^3 for the 20% SBS foam, whereas the improvement was slight when the $CaCO_3$ content was below 5%; this indicated that the nucleation effect was limited at low $CaCO_3$ concentrations. However, the cell density jumped to 21.4×10^6 cells/cm^3 when the $CaCO_3$ content reached 5%. There were two reasons for the cell diameter diminution and cell density increase. First, the $CaCO_3$ particles acted as nucleation sites; this reduced the critical energy barrier for the initial bubble to nucleate according to the widely

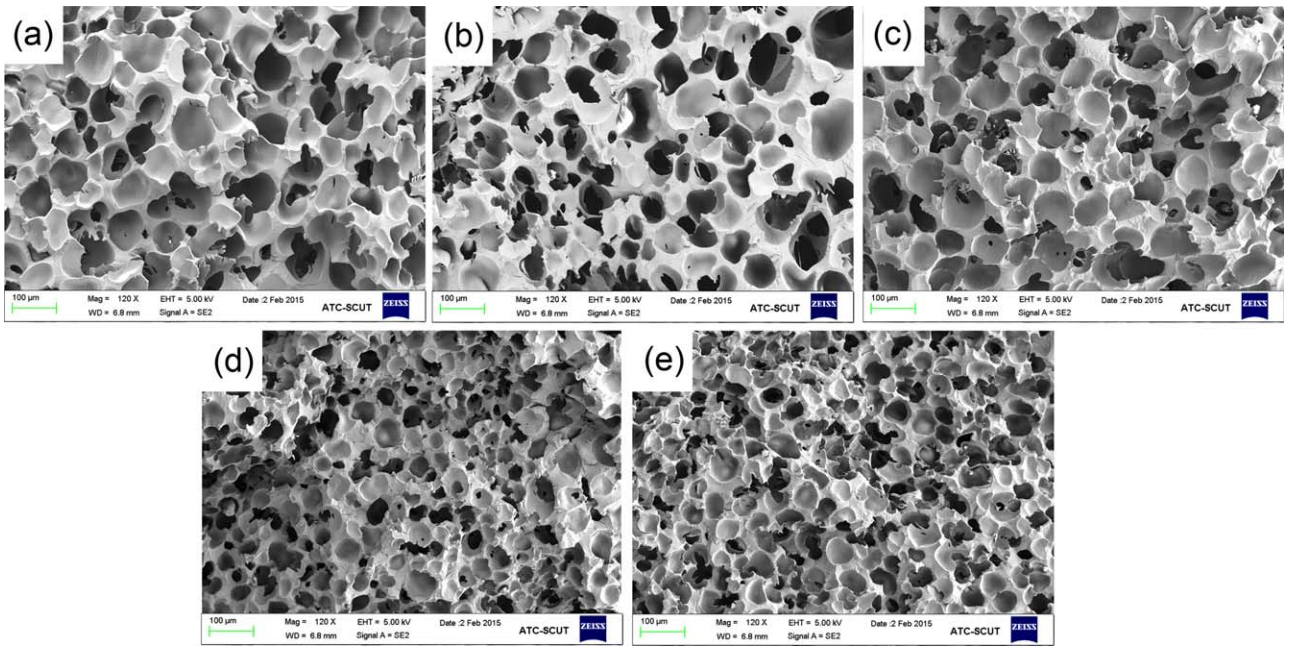

Figure 9. SEM images of the extrusion-foamed samples: (a) PS/SBS, (b) 1% $CaCO_3$, (c) 3% $CaCO_3$, (d) 5% $CaCO_3$, and (e) 10% $CaCO_3$. [Color figure can be viewed in the online issue, which is available at wileyonlinelibrary.com.]

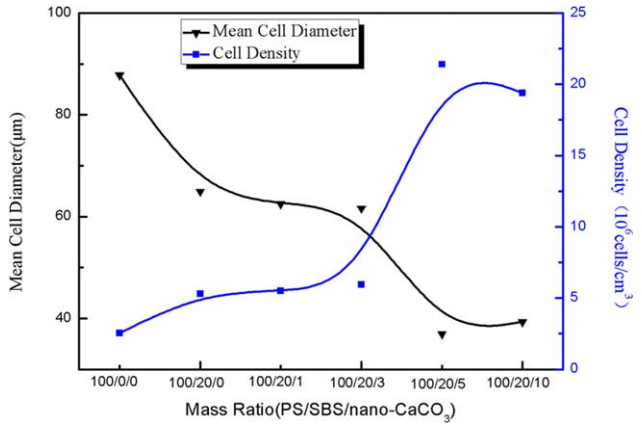

Figure 10. Statistical results for the mean cell diameter and cell density of the PS/SBS and PS/SBS/$CaCO_3$ nanocomposites. [Color figure can be viewed in the online issue, which is available at wileyonlinelibrary.com.]

acknowledged nucleation theory in foaming. Second, the addition of $CaCO_3$ particles significantly enhanced the system viscosity; this caused the higher surface tension that the bubble needed to overcome to expand; hence, smaller cells were obtained. Noticeably, the cell density was reduced and the cell diameter was increased for the 10% $CaCO_3$ foam; this was attributed to the aggregation of $CaCO_3$ nanoparticles and the reduction in the system viscosity, as presented in Figures 7 and 8. The $CaCO_3$ aggregation spots increased obviously when the $CaCO_3$ content was higher than 5%. This indicated that the nucleation effect decreased as the $CaCO_3$ content increased further; this explained the decrease in the cell density. Meanwhile, the system viscosity for the 10% $CaCO_3$ composite was lower than that of the 5% $CaCO_3$ composite; this indicated a lower surface tension for cells to expand. These resulted in an increase in the cell diameter.

Compressive Properties of the PS, PS/SBS Blends, and PS/SBS/$CaCO_3$ Nanocomposites

Although microcellular foams possess multiple advantages, such as a light weight, cost savings, low energy cost, high heat, and sound-barrier effects, their significant disadvantages, which sacrificed the mechanical strength, were recognized as the main reason for limitations in the wide application of microcellular foams.[38] Therefore, researchers have been working on improving the mechanical performance of microcellular foams for decades. There are basically two approaches for enhancing the mechanical properties of polymer foams: changing the microcell structure and modifying the matrix material system. It has been reported that when the cells are finer, better mechanical properties in the foams will be achieved.[37] Some researchers have reported that microcells with fine cell structures acted just as rubbery additives; this significantly enhanced the impact strength of the materials.[39,40] However, the tensile and compressive properties of the foams were relatively hard to improve because of the defects created by the voids inside of the foams.

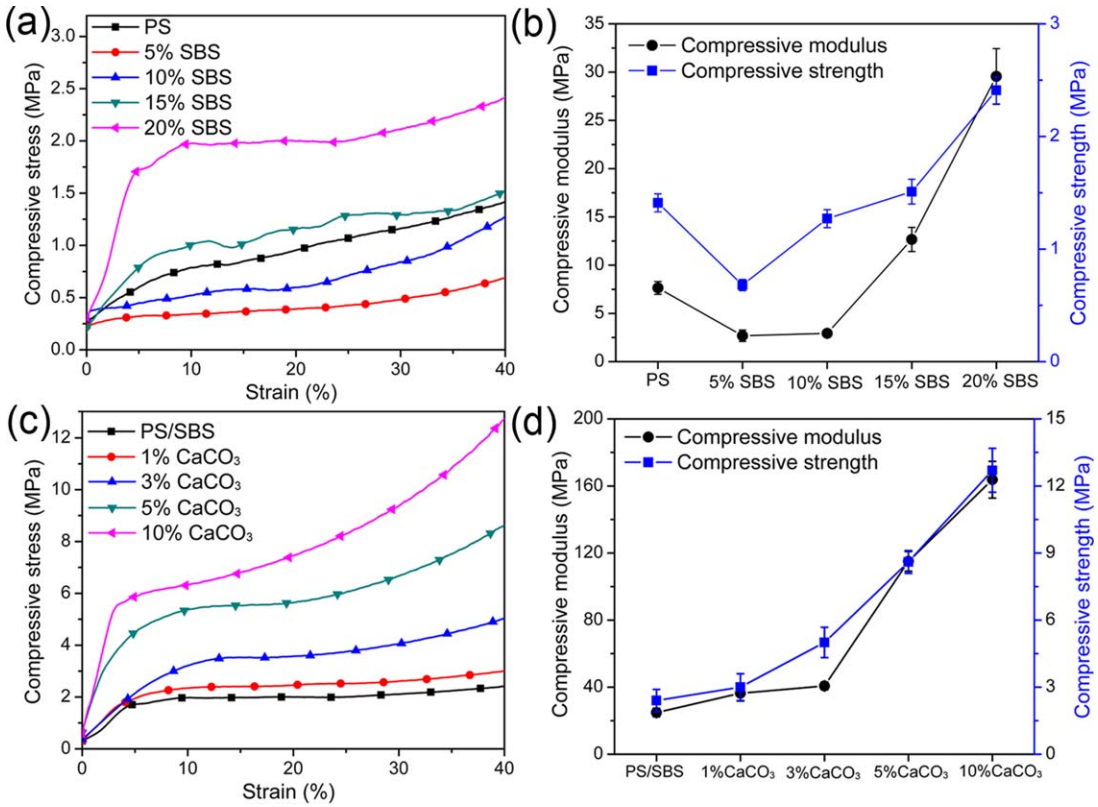

Figure 11. Compressive properties of the (a,b) extrusion-foamed PS/SBS blends and (c,d) extrusion-foamed PS/SBS/$CaCO_3$ nanocomposites: (a,c) compressive stress–strain curves and (b,d) statistical results for the compressive modulus and strength. [Color figure can be viewed in the online issue, which is available at wileyonlinelibrary.com.]

In this study, the compressive properties of the PS/SBS blends and PS/SBS/$CaCO_3$ nanocomposites extrusion foams were investigated in detail. The compressive test results of the extrusion foams are shown in Figure 11. As shown in Figure 11(a), it was interesting that the compression properties of the PS/SBS blends were reduced when the SBS content was lower than 15%, and it was improved when the SBS content exceeded 15%. According to the statistical results [Figure 11(b)], the compressive modulus and compressive strength at 40% strain of the 20% SBS foams were 289.5 and 70.9% higher than that of the neat PS foams, respectively. The trend of compressive test results as the SBS content increased was found to correlate very well with the cell morphology results. This indicated that the reduced cell size and significantly enhanced cell density of the PS/SBS foams at high SBS contents (e.g., 15 and 20%) and caused the improvement in the compression properties of the foams; it further implied that the positive effect of the cell structure refinement overwhelmed the negative effect of the compressive properties sacrificed by SBS. These might have occurred because the smaller and denser cells in the foams more effectively dissipate local stress than larger cells under an external force.

To further investigate the effects of additional blowing agents on the compressive properties of the extrusion foams, $CaCO_3$ nanoparticles were added to the PS/SBS system with 20% SBS content at various loading concentrations. According to Figure 11(c), it was clearly observed that the compressive curves of the extrusion foams with higher $CaCO_3$ concentration located higher. The statistical results [Figure 11(d)] indicated a significant improvement in the compressive properties for the PS/SBS/$CaCO_3$ nanocomposites. This improvement was attributed to two factors, which are smaller and denser cells and the rigidity provided by the $CaCO_3$ nanoparticles. When the $CaCO_3$ content was less than 3%, the compressive property improvement was slight because of the delicate enhanced cell density. However, the compressive modulus of the 5% $CaCO_3$ foams was found to be 379.2% higher than that of PS/SBS foams with 20% SBS because of the largely enhanced cell density and $CaCO_3$ concentration. As shown in Figure 10, we found that the cell density of the 10% $CaCO_3$ foam was lower than that of the 5% $CaCO_3$ foam because of the particle aggregation at a high concentration; however, its compressive properties were still superior to those of the 5% $CaCO_3$ foam, as shown in Figure 11(d). This might have been because the excessive $CaCO_3$ particles acted as not only nucleation agents but also a component of the material system, and this provided a significant compressive property improvement.

Therefore, in this study, we prepared PS/SBS blends and PS/SBS/$CaCO_3$ nanocomposites and produced microcellular foams via extrusion foaming with SC-CO_2 as the blowing agent. The cell evolution behavior and the mechanical properties of the foams as the material components were changed were investigated comprehensively for the first time. We were able to control the cell size and cell density of the extrusion foams and enhance the compressive properties of the foams through variations in the SBS content and $CaCO_3$ concentration. The theoretical discussion and outcomes of this study would be useful in industrial applications where SBS-toughened and $CaCO_3$-reinforced PS foams with light weights and high mechanical performance are needed.

CONCLUSIONS

In this study, PS/SBS binary blends and PS/SBS/$CaCO_3$ ternary nanocomposites with various compositions were prepared by melt compounding and subsequent extrusion foaming with SC-CO_2 as a physical blowing agent to investigate the cell evolution behavior and compressive properties of the SBS-toughened and $CaCO_3$-reinforced PS foams. The phase morphology results suggest good compatibility between the PS and SBS, and $CaCO_3$ nanoparticles were added to the PS/SBS matrix without showing obvious aggregation at concentrations below 5 wt %. The addition of SBS and $CaCO_3$ nanoparticles both improved the rheological properties of the system. The cell morphology of the extrusion foamed samples was found to correlate well with the viscosity results at low frequency. The cell diameter increased when the SBS content was 5% and then decreased as the SBS content was increased further. The 20% SBS sample showed the smallest cell diameter of 64.9 μm. The addition of $CaCO_3$ to the 20% SBS blends further improved the cell density and reduced the cell size through the nucleation effect of the nanoparticles. The compression test results reveal that the compressive properties of PS were significantly enhanced when the cell size diminished and rigid nanofiller (e.g., $CaCO_3$ nanoparticles) was added, regardless of the softening effect of SBS. The compressive modulus for 5% SBS foam was lower than that of neat PS, whereas it was 289.5% higher than that of the neat PS for 20% SBS foam. The compressive modulus was further enhanced by 379.2% after the addition of 5% $CaCO_3$ to the PS/SBS blends. Therefore, we were able to produce PS/SBS/$CaCO_3$ foams with a fine cell size, high cell density, and excellent compressive properties. These may be suitable for high-performance applications.

ACKNOWLEDGMENTS

The authors acknowledge the financial support of the National Science Foundation of China (contract grant numbers 21174044, 51573063, and 51503069), the Guangdong Nature Science Foundation (contract grant numbers S2013020013855 and 9151064101000066), National Basic Research Development Program 973 in China (contract grant number 2012CB025902), the Fundamental Research Funds for the Central Universities (contract grant numbers 2015ZM093 and 2015ZM099), and the State Key Laboratory of Materials Processing and Die & Mold Technology, Huazhong University of Science and Technology (contract grant number P2016-10).

REFERENCES

1. Fu, J.; Jo, C.; Naguib, H. E. *Cell. Polym.* **2005**, *24*, 177.
2. Matuana, L. M.; Park, C. B.; Balatinecz, J. J. *Cell. Polym.* **1998**, *17*, 1.
3. Maharsia, R. R.; Jerro, H. D. *Mater. Sci. Eng. A* **2007**, *454*, 416.

4. Lee, J. W. S.; Wang, J.; Yoon, J. D.; Park, C. B. *Ind. Eng. Chem. Res.* **2008**, *47*, 9457.
5. Pasricha, A.; Wing, G.; Kumar, O.; Tuttle, M.; Seeler, K. *Polym. Eng. Sci.* **2005**, *45*, 1639.
6. Ding, J.; Shangguan, J. N.; Ma, W. H.; Zhong, Q. *J. Appl. Polym. Sci.* **2013**, *128*, 3639.
7. Siripurapu, S.; DeSimone, J. M.; Khan, S. A.; Spontak, R. *J. Adv. Mater.* **2004**, *16*, 989.
8. Avella, M.; Cocca, M.; Errico, M. E.; Gentile, G. *J. Cell. Plast.* **2011**, *47*, 271.
9. Milleret, V.; Bittermann, A. G.; Mayer, D.; Hall, H. *Materials* **2009**, *2*, 292.
10. Zhai, W. T.; Kuboki, T.; Wang, L. L.; Park, C. B.; Lee, E. K.; Naguib, H. E. *Ind. Eng. Chem. Res.* **2010**, *49*, 9834.
11. Taki, K.; Nitta, K.; Kihara, S.; Ohshima, M. *J. Appl. Polym. Sci.* **2005**, *97*, 1899.
12. Kawazura, T.; Chaikumpollert, O.; Kawahara, S. *Chin. J. Polym. Sci.* **2013**, *31*, 1424.
13. Saengthaveep, S.; Magaraphan, R. *Adv. Polym. Technol.* **2013**, *32*, 21352.
14. Yousefi, A. A. *J. Appl. Polym. Sci.* **2013**, *127*, 659.
15. Tsai, Y.; Wu, J. H.; Li, C. H.; Wu, Y. T.; Leu, M. T. *J. Appl. Polym. Sci.* **2010**, *116*, 172.
16. Boyanova, M.; Calleja, F. J. B.; Fakirov, S. *J. Mater. Sci. Lett.* **2003**, *22*, 1741.
17. Mohammady, S. Z.; Mansour, A. A.; Knoll, K.; Stoll, B. *Polymer* **2002**, *43*, 2467.
18. Adhikari, R.; Huy, T. A.; Henning, S.; Michler, G. H.; Knoll, K. *Colloid Polym. Sci.* **2004**, *282*, 1381.
19. Fang, Z. P.; Guo, Z. H.; Zha, L. L. *Macromol. Mater. Eng.* **2004**, *289*, 743.
20. Thomann, Y.; Thomann, R.; Hasenhindl, A.; Mulhaupt, R.; Heck, B.; Knoll, K.; Steininger, H.; Saalwachter, K. *Macromolecules* **2009**, *42*, 5684.
21. Chen, D. Z.; Yang, H. Y.; He, P. S.; Zhang, W. A. *Compos. Sci. Technol.* **2005**, *65*, 1593.
22. Wang, Z. B.; Li, G. C.; Peng, H. R.; Zhang, Z. K.; Wang, X. *J. Mater. Sci.* **2005**, *40*, 6433.
23. Amr, I. T.; Al-Amer, A.; Thomas, S.; Al-Harthi, M.; Girei, S. A.; Sougrat, R.; Atieh, M. A. *Compos. B* **2011**, *42*, 1554.
24. Kim, T. H.; Lim, S. T.; Lee, C. H.; Choi, H. J.; Jhon, M. S. *J. Appl. Polym. Sci.* **2003**, *87*, 2106.
25. Yeo, S. S.; Hsuan, Y. G. *Geosynthetics* **2006**, *1*, 1639.
26. Lu, M.; He, B.; Wang, L. S.; Ge, W.; Lu, Q. Y.; Liu, Y. K.; Zhang, L. *Q. Compos. B* **2012**, *43*, 50.
27. Ruamcharoen, J.; Ratana, T.; Ruamcharoen, P. *Polym. Eng. Sci.* **2014**, *54*, 1436.
28. Siengchin, S.; Karger-Kocsis, J. *Compos. B* **2013**, *45*, 1458.
29. Weon, J. I.; Sue, H. J. *J. Mater. Sci.* **2006**, *41*, 2291.
30. Sun, Q. J.; Xi, T. T.; Li, Y.; Xiong, L. *PLoS One* **2014**, *9*, e0106727.
31. Chiu, F. C.; Lai, S. M.; Wong, C. M.; Chang, C. H. *J. Appl. Polym. Sci.* **2006**, *102*, 2276.
32. Hua, Y.; Gu, L.; Premaraj, S.; Zhang, X. *Materials* **2015**, *8*, 3519.
33. Yuan, S. Y.; Du, L. Y.; Zheng, G.; Huang, R. *Acta Polym. Sin.* **2004**, 478.
34. Wang, J.; Cheng, X. G.; Yuan, M. J.; He, J. S. *Polymer* **2001**, *42*, 8265.
35. Huang, H. X.; Wang, J. K. *J. Appl. Polym. Sci.* **2007**, *106*, 505.
36. Kiss, A.; Fekete, E.; Pukanszky, B. *Compos. Sci. Technol.* **2007**, *67*, 1574.
37. Rachtanapun, P.; Selke, S. E. M.; Matuana, L. M. *J. Appl. Polym. Sci.* **2003**, *88*, 2842.
38. Siripurapu, S.; Gay, Y. J.; Royer, J. R.; DeSimone, J. M.; Spontak, R. J.; Khan, S. *A. Polymer* **2002**, *43*, 5511.
39. Zhang, H. B.; Yan, Q.; Zheng, W. G.; He, Z. X.; Yu, Z. Z. *ACS Appl. Mater. Interfaces* **2011**, *3*, 918.
40. Sun, X.; Kharbas, H.; Peng, J.; Turng, L. S. *Polymer* **2015**, *56*, 102.